

# Numerical Study of Heat Transfer on a Dimpled Surface with CEDRE code

*Ph. Grenard ; V. Quintilla-Larroya ; E. Laroche  
Office National d'Etudes et de Recherches Aéronautiques  
29 avenue de la Division Leclerc, 92322 Châtillon, France*

May 2007

## Abstract

This article presents the numerical study performed with the CEDRE code, developed at ONERA, to predict heat transfer on a dimpled surface placed on one wall of a rectangular channel. Various models of turbulence are tested on three basic configurations. The comparison between numerical results and experimental Nusselt profiles shows that the  $k - \varepsilon$  model implemented in CEDRE is the most appropriate to predict heat transfer. A parametric study is performed with this turbulence model to determine the effects of Reynolds number, dimple depth and dimple shape on heat transfer enhancement and pressure drop. Finally, the technologies using dimples and ribs are compared in term of thermal performance.

## 1. Introduction

Various techniques are employed to enhance convective heat transfer rates in gas turbine engine passages used for internal cooling of turbine airfoils. These include protruding ribs arranged in periodic patterns in the internal cooling passages, and short pin-fins implemented instead of ribs in the trailing section of the blade. These devices promote turbulent mixing in the bulk flow and enhance the heat transfer capability in the cooling channel. The main drawback of these technologies is the significant pressure drag produced by the rib or pin fin protrusion into the flow. The pressure loss induced contributes to raise the compressor load and to deteriorate the engine aerodynamics and the cycle efficiency. In this context, the technology using concavities (dimples) recently attracted interest due to the substantial heat transfer augmentations it induces, with pressure drop penalties smaller than with other types of heat augmentation devices. Convective heat transfer and pressure drop for turbulent airflow in a rectangular channel with a dimpled wall have already been investigated by many authors. The influence of Reynolds number [1], inlet stagnation temperature to surface temperature ratio [1], longitudinal turbulence intensity [2], channel height [1] and dimple geometry (depth [3] and shape [4, 5]) has been characterized. Visualizations with smoke generated from multiple wires have also been performed to better understand the structure of the flow on and above the dimpled surface [6]. From a numerical point of view, fewer studies are available. Lin et al. [7] provide computational results with the  $k - \omega$  turbulence model for a high aspect ratio channel, in which the walls are lined with four rows of hemispherical cavities arranged in a staggered fashion. Flow streamlines and temperature distributions are presented that provide insight into the flow structural characteristics produced by the dimples. More recently, Park et al. [8, 9] and Won et al. [10] have performed simulations with the FLUENT code to determine the flow structure and the influence of the dimple depth and shape on heat transfer considering the experimental configuration of Burgess et al. [3]. As a result, heat transfer augmentation patterns and values predicted numerically are not in good agreement with the experimental data issued from the literature. The present paper also deals with the numerical prediction of heat transfer and pressure drop in a rectangular dimpled channel. In a first part, the computational methodology including the presentation of the CEDRE code, the basic configurations tested and the numerical schemes and models are presented. Then, a parametric study is performed to characterize numerically the effects of Reynolds number, channel height, dimple depth and shape on heat transfer. In a final part, the two technologies using dimples and ribs are compared in term of thermal performance.

## 2. Computational methodology

### 2.1 The CFD code CEDRE

The CEDRE code is a 3D solver of the Reynolds Averaged Navier Stokes equations based on the finite volume formulation. This code is multisolver to take into account multiphysic phenomena such as multispecies, turbulent and reactive flow ; dispersed phase (Lagrangian and Eulerian formulation) ; convection/diffusion and radiation (Monte Carlo approach). It uses multidomain techniques on generally unstructured meshes. Various numerical schemes are available for time integration (implicit and explicit methods) and spatial approximation (discretization of second order with approximate Riemann solvers). This code is also fully parallel with MPI instructions to manage the parallel processing. It is adapted to all architectures (parallel, superscalar).

### 2.2 Basic Configurations

Three basic configurations, for which experimental data exist, are considered to validate the numerical parameters and physical models of the CEDRE code. These configurations consist in rectangular channels with twenty rows of half hemispherical dimples arranged in a staggered fashion (figure 1). The common parameters between these three geometries are the following ones:  $D = 5.08$  cm,  $p_x = p_y = 8.22$  cm (figure 2). The length of the computational area is of 1 m and the distance between the channel inlet and the first dimple center measures 15 cm.

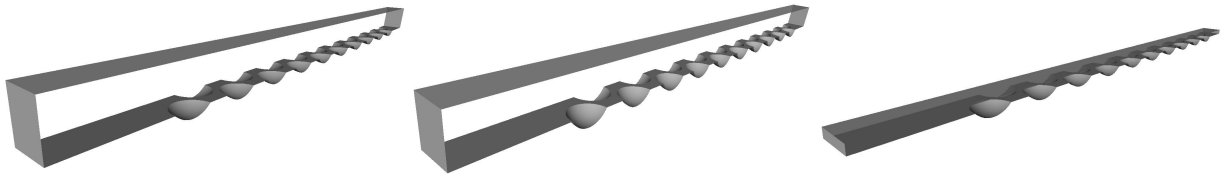


Figure 1: Geometry of the three basic configurations

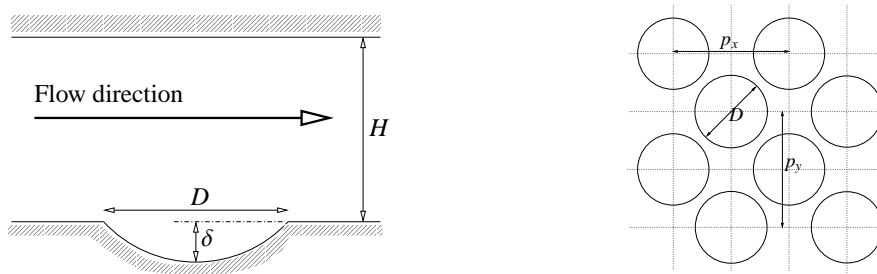


Figure 2: Geometric parameters characterizing the array of dimples

These configurations differ from the value of the channel height and the dimple depth. The first case corresponds to a reference one for which the channel height is quite large to avoid the influence of the upper wall. For the second case, deeper cavities are considered with a channel height unchanged. In the last configuration, the dimple depth is equal to the reference one and the channel height is 5 times smaller than the one considered for the two previous cases. These geometric parameters are summarized in table 1.

Table 1:  $H/D$  and  $\delta/D$  ratio of the three basic configurations

	$H/D$	$\delta/D$
Case 1	1	0.2
Case 2	1	0.3
Case 3	0.2	0.2

The meshes relative to the three basic configurations are composed of tetrahedral elements, except near the walls

where prisms are considered to describe more accurately the boundary layers. CENTAUR is used for the development of these computational grids, whose characteristics are summarized in table 2.

Table 2: Meshes characteristics

	Number of Nodes	Nuber of Faces	Number of Cells
Case 1	205365	953146	384723
Case 2	223405	1031875	415703
Case 3	261261	1607159	708817

## 2.3 Boudary conditions, models and numerical schemes

### 2.3.1 Boundary conditions

A uniform velocity profile is employed at the inlet of the smooth portion of the duct. An inlet turbulence intensity level of about 10% is used, and the turbulent length scale at the inlet is taken equal to a tenth of the channel height. A constant heat flux of  $650 \text{ W/m}^2$  is applied on the dimpled surface, which leads to an inlet stagnation temperature to surface temperature ratio  $T_{oi}/T_w$  of 0.95. On the upper wall, temperature is constant and equal to the inlet one (300 K). All results for the basic configurations are obtained for a Reynolds number based on channel height of 20 000. At the exit of the computational domain, a pressure of 1 bar is imposed.

### 2.3.2 Models and numerical schemes

Ideal gas air is used as the working fluid. Turbulence properties are calculated considering the  $k - \varepsilon$  turbulence model governed by transport equations. The Reynolds averaged Navier Stokes equations are solved numerically in conjunction with the turbulent transport equations. Near wall regions are fully resolved for  $y^+$  values less than 1. In these regions, low Reynolds corrections are taken into account and no wall functions are utilized.

## 2.4 Results and discussion

The goal of these three computations is to assess the ability of the CEDRE code and the turbulence model chosen to predict heat transfer on the dimpled surface. The three configurations considered (described in table 2) correspond to those with most detailed experimental results available.

### 2.4.1 Evaluation of baseline Nusselt number

The baseline Nusselt number  $Nu_0$  is extrapolated from the Nusselt number on the first smooth part of the computed channel. This choice was made to have the same approach as the experiments where  $Nu_0$  is extracted from a smooth channel experiment and not from a correlation. The smooth part of the channel is about 15 cm long, which is not enough to have a fully developed flow, but Nusselt number tends to an asymptotic behavior. This asymptotic Nusselt number is taken as the baseline Nusselt number. This evaluation is not the most accurate one, but it has the advantage to give a baseline Nusselt number and according Nusselt field on the same computation. An example is provided on figure 4

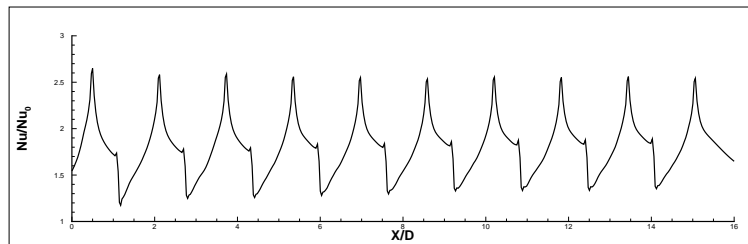


Figure 3: Periodicity of the Nusselt number in computations for the baseline case 1

**2.4.2 Case 1 :  $H/D = 1$  and  $\delta/D = 0.2$**

This is the baseline configuration for which precise experimental results are available. As the computation deals with a limited number of dimples, the periodic behaviour of the Nusselt number on the dimpled plate has been verified on this case (fig. 3). For this geometry, experimental results are given by Ligrani and Mahmood [1, 11]. An important point is that the surface used to calculate the heat flux on the dimpled plate is not the same on these two studies, as in [11] the projected flat surface was used unlike in [1] where the total surface was used. This gives a 16.4% overestimations for the results obtained with the flat surface, as stated in [1]. In our computations, the heat flux is numerically imposed on every surface cell. Thus the most appropriate results for comparison are those which take the full surface [1]. Four profiles are shown in figures 6 and 7 and the cutting planes are presented in figure 5.

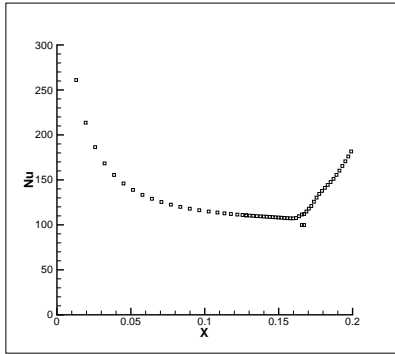


Figure 4: Evolution of the Nusselt number in the first smooth part of the channel for the baseline case 1

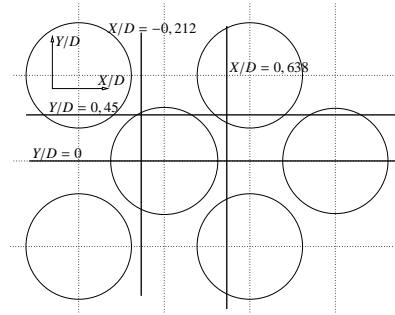


Figure 5: Locations of the cutting planes in X and Y directions

The results obtained by our computations fits quite well for the mean Nusselt value for each of these profiles. It also predicts reasonably well the shape of those profiles. For example, on the  $Y/D = 0$  profile, corresponding to the symmetry plane of the geometry, computation and experiments give similar results. One can see the Nusselt drop when entering the dimple ( $X/D = 7.591$ ) due to the recirculation zone where the fluid loses some of its cooling effectiveness, and the peak value of Nusselt at the exit of the dimple ( $X/D = 8.591$ ). The computations seem to flatten the profiles, to underestimate the peak value and to overpredict the lower value of the Nusselt number.

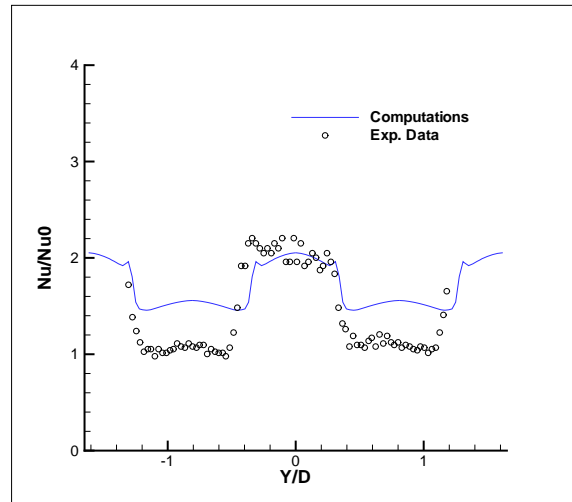
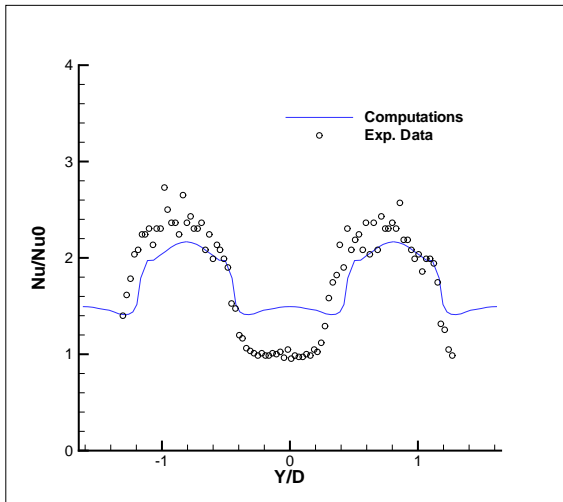


Figure 6: Nusselt Number for  $X/D = -0.212$  (left) and  $X/D = 0.638$  (right)

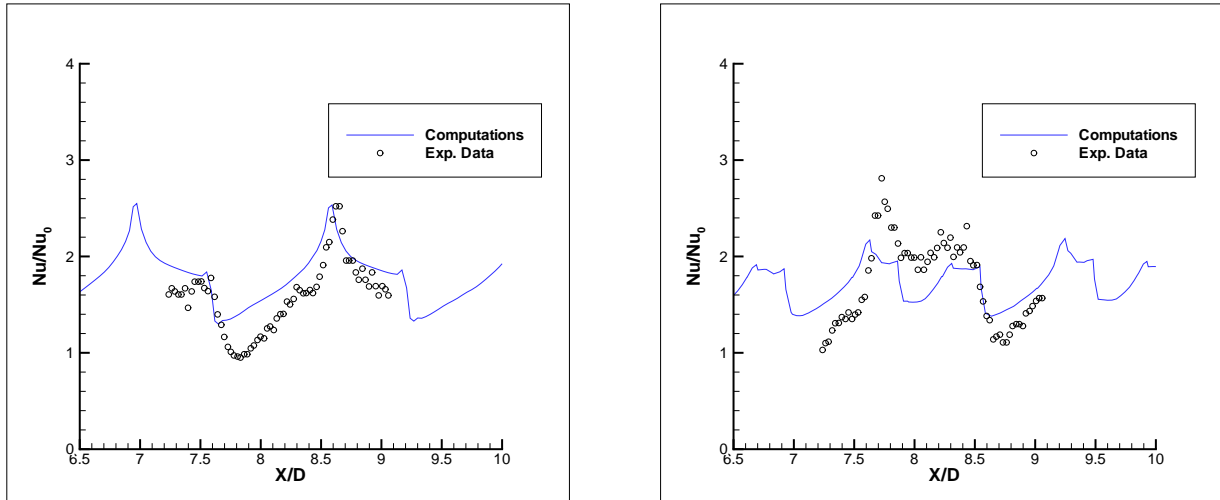


Figure 7: Nusselt Number for  $Y/D = 0$  (left) and  $Y/D = 0.45$  (right)

### 2.4.3 Case 2 : $H/D = 1$ and $\delta/D = 0.3$

This case corresponds to deeper dimples. For this configurations, experimental results are obtained from [3] and consists of one profile and one Nusselt number field. The reader has to be aware that for these experimental results, the area used to evaluate heat fluxes is the projected plane surface. Thus, as stated before, a corrected value (lessened by 16.4%) is also proposed with the computational results on figure 8. Once again the mean value of the Nusselt number is well predicted by the code. Even the drop level is reasonably well predicted by the computation. But the second part of the curve (second half of the dimple and after dimple behaviour) is underestimated and seems too smooth compared to experimental values. However, we can observe that the experimental results do not appear to be periodic. In fact, we should observe the same pattern for  $7.2 < X/D < 8.2$  and  $8.8 < X/D < 9.8$ , which is obviously not the case on the experimental data unlike on the computational results.

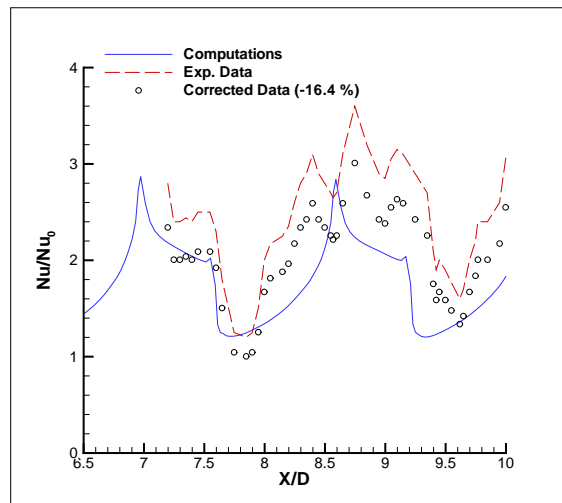


Figure 8: Nusselt Number for  $Y/D = 0$

In order to complete the study of this case, three Nusselt number fields are presented on figure 9. The first one, on the left, is the experimental field obtained by Burgess [3], the second one (center) is the FLUENT result from Park, Desam and Ligrani [8], and the last one on the right is from the current CEDRE computation. As done by Park, Desam and Ligrani, the color scale has been changed compared to experimental results in order to observe the aspect of the Nusselt repartition on the dimpled surface. The first remark is that the maximum value of the Nusselt number from CEDRE computations on this case seems a little higher than the FLUENT ones, but still far from the experimental

levels. The second remark is about the aspect of the Nusselt repartition. On the experimental field, there is a unique low Nusselt number zone at the entrance of the dimple, which extends next to the center of the dimple on the dimple sides (white zone of the first image on figure 9). This behaviour is not retrieved at all by the FLUENT computation unlike in the current results where the "crescent moon" aspect even if it is not as marked as in the experiments. At the exit of the dimple, experimental field shows a peak value behind the dimple (on the symmetry axis) which is retrieved on the CEDRE computation. On the FLUENT calculation, there are two peak value which are not on the symmetry axis but in the direction of the dimples of the next row.

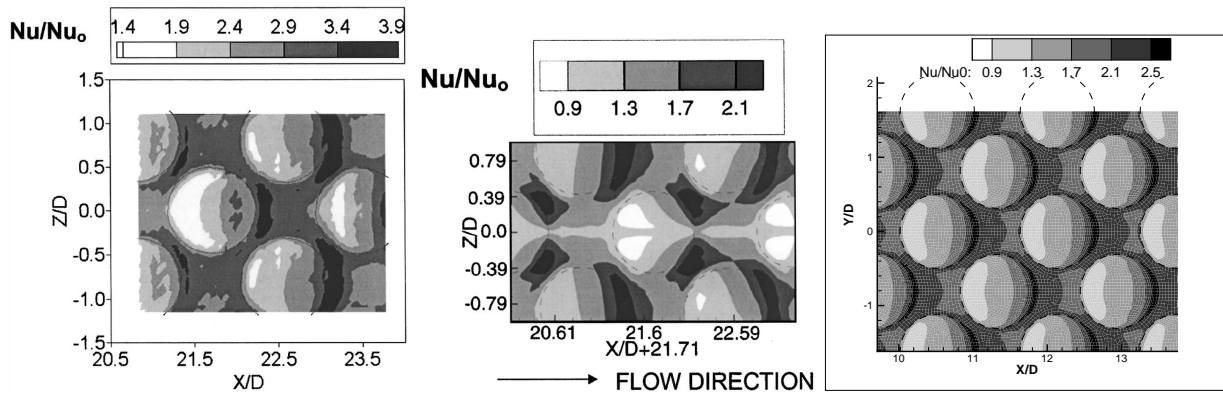


Figure 9: Nusselt number repartition : Experiments (left), FLUENT computation (center), CEDRE computation (right)

**2.4.4 Case 3 :  $H/D = 0.2$  and  $\delta/D = 0.2$**

For this case, four profiles are available and are presented on figure 10 and 11. On the symmetry plane of the geometry computations and experimental data are in good agreement, even if the low Nusselt region seems smaller on the computational result. The same observation as case 1 and case 2 is made on the three other profiles, that is a phenomenology recovered by the computations, but the magnitude of the profile is significantly larger on experimental data. Once again, on the  $X/D$  constant profiles, experimental data are not exactly symmetric for  $X/D = -0.212$ . Another surprising observation can be made on the figure 10, where the two profiles presented should be approximately the same, as they correspond to the same type of zone observed for two staggered dimples : the  $X/D = 0.638$  profile should nearly be a translation of  $Y/D = \pm 0.819$  of the  $X/D = -0.212$  profile due to the symmetry of the geometry studied. This is not the case, not only for the Nusselt number levels, but also for the shape of the profile. Compared to the first profile on figure 11, the value at  $Y/D = 0$  and just after the dimple ( $X/D = 0.638$ ) seems to comfort the  $X/D = 0.638$  experimental profile, which is moreover completely symmetric as awaited. The  $X/D = -0.212$  profile seems to be a little suspicious for the moment. It must also be reminded that this case is really interesting to compute because of the strong interaction between the upper wall and flow structure, which can lead to absurd results. This seems to be a good dimensionnal computation case.

**2.4.5 Conclusion on baselines cases**

The CEDRE code is able to predict quite well, at least on these three cases, the shape of the Nusselt number repartition on the dimpled plate. However the magnitude of these Nusselt number seems underestimated, even if the mean value is in good agreement with the experimental data. After having computed these three baseline cases, it has been decided to evaluate the influence of several geometrical and physical parameters on the Nusselt number repartition.

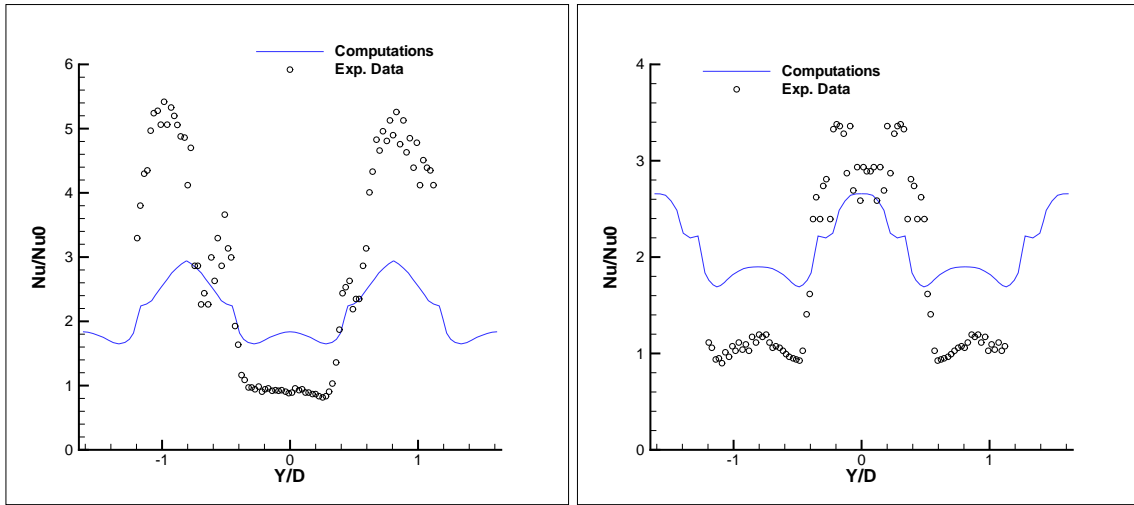


Figure 10: Nusselt Number for  $X/D = -0.212$  (left) and  $X/D = 0.638$  (right)

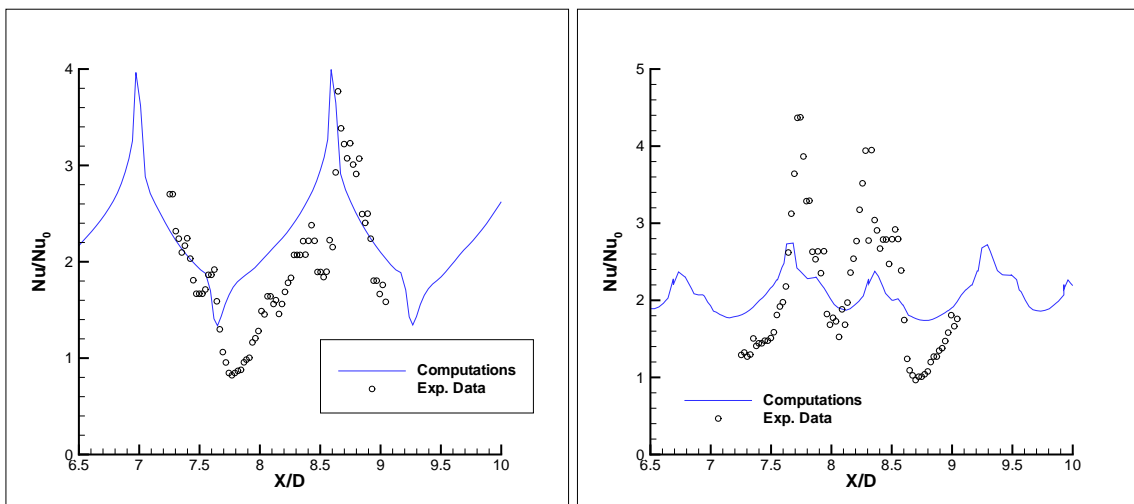


Figure 11: Nusselt Number for  $Y/D = 0$  (left) and  $Y/D = 0.45$  (right)

### 3. Parametric Study

#### 3.1 Effect of Reynolds Number

As mentioned in the state of the art, the influence of Reynolds number is neglectable on the Nusselt number behaviour on dimpled surfaces (at least in a reasonable range of Reynolds). To test this behaviour numerically, three cases were computed. The baseline case 1 (presented before) with a Reynolds number of 20 000 and two other Reynolds numbers on the same geometry (10 000 and 50 000) which correspond to bulk velocity ranging from 7 to 35  $m/s$ . As presented in figure 12, there is nearly no influence of the Reynolds number. When looking more precisely, the computations show a little effect which is a higher Nusselt number value obtained for the higher Reynolds number. However, the difference is quite small as the friction can significantly grow. Thus a high Reynolds number is not a good compromise for this type of cooling device.

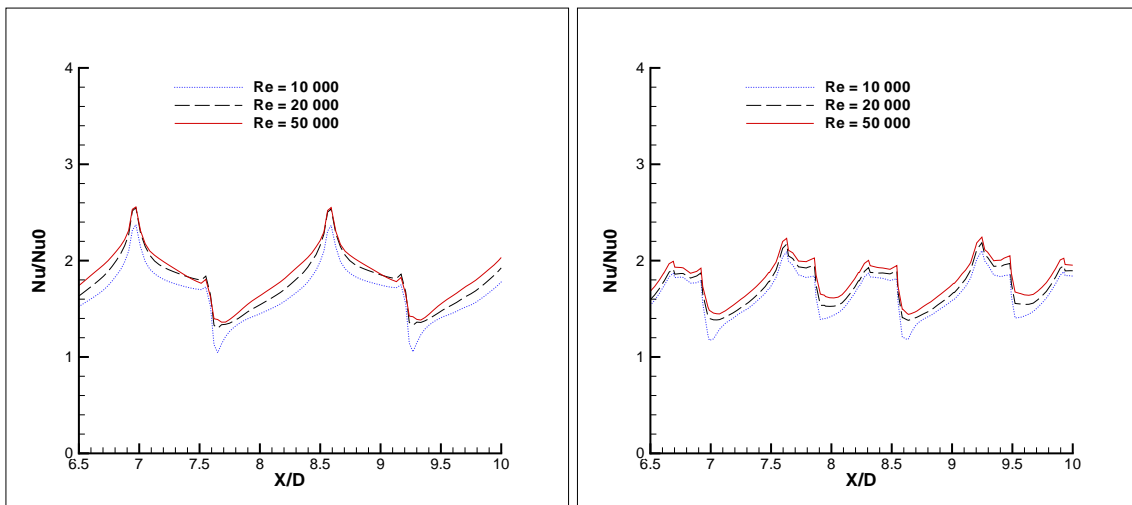


Figure 12: Nusselt Number for different Reynolds number. Left :  $Y/D = 0$  ; Right :  $Y/D = 0.45$

#### 3.2 Effect of dimple depth

An important geometric parameter is the depth of the dimple. In fact, a deeper dimple can better promote the turbulence mixing and thus the cooling. However, a too deep dimple can cause a large recirculation at its entrance and then reduce its cooling properties. For this influence, three cases have been computed on a  $H/D = 1$  channel, for  $\delta/D = 0.1$  ; 0.2 and 0.3 . These two last cases have been presented before (cases 1 and 2 of the baselines cases). On the figure 13 the Nusselt number repartitions are presented for these three cases. The  $\delta/D = 0.1$  case is quite similar to a flat plate where the variations of the Nusselt number are really limited : this case is not a good turbulence promoter and is not efficient for cooling the wall. On the opposite, the  $\delta/D = 0.3$  case, compared to the  $\delta/D = 0.2$  case, presents a higher value for the Nusselt number behind dimples, but at the same time a larger recirculation zone inside the dimple which gives a globally lower Nusselt number inside the dimples. Moreover, a deeper dimple can provoke a higher pressure loss in the channel. At last, for mechanical properties of the material, it is better to have a more uniform field of Nusselt. For all these reasons, it does not seem to be useful to raise the adimensionned dimple depth above a value of approximatively 0.2 .

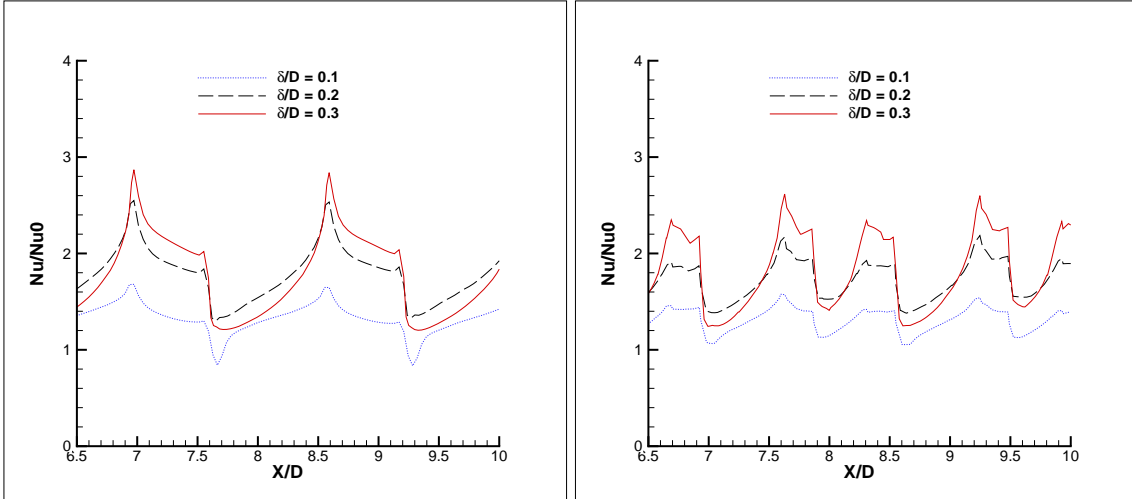


Figure 13: Nusselt Number for different dimple depth. Left :  $Y/D = 0$  ; Right :  $Y/D = 0.45$

### 3.3 Effect of dimple shape

Two other shapes of dimples have also been computed : a cylinder and an inclined half-cylinder with a non-dimensional depth of  $\delta/D = 0.2$  . These geometries and their parameters are represented on the figure 14 and compared to the baseline case 1. The computationnal domain is represented on the figure 15 and results are given in term of Nusselt number field. On the cylinder shaped dimple, a strong recirculation, inducing pressure loss and thermal penalties, is

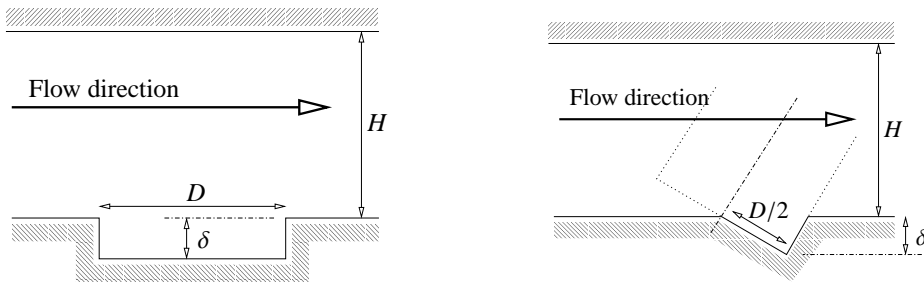


Figure 14: Cylinder and half-cylinder dimples.

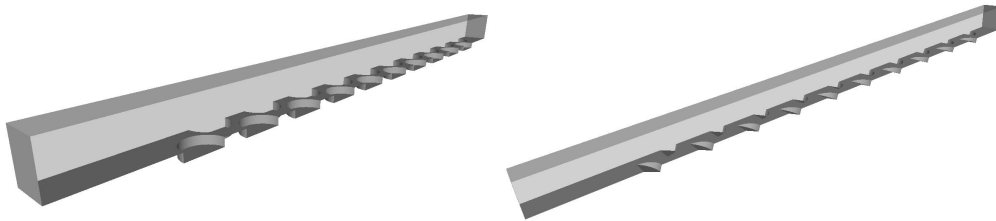


Figure 15: Computational domain. Cylinder (left), half cylinder (right)

observed inside the dimple. Compared to the spherical shaped dimple of same depth, this cylindrical geometry induces hot spots and strong recirculation zones. Thus it is advised to prefer spherical shaped dimples to cylindrical ones. The idea of the second shape tested during this work comes from this observation : to maximize the cooling properties of the dimple, we have to limit the recirculation created at its entrance while keeping a strong turbulence promoter at the exit. As shown on figure 16, there still exists a low Nusselt number zone inside the dimple, but also two high Nusselt number zones at the exit of the dimple. This sort of shape is also interesting because of its geometry, the density of dimples

on the surface could be increased. As stated above, there is still a recirculation in the dimple which induces penalties on the cooling properties. A further improvement would probably consists in reducing this half cylinder dimple depth and/or transforming the circular base to an elliptic one in order to stretch the dimple along the flow direction to limit at a minimum the entrance effect in the dimples.

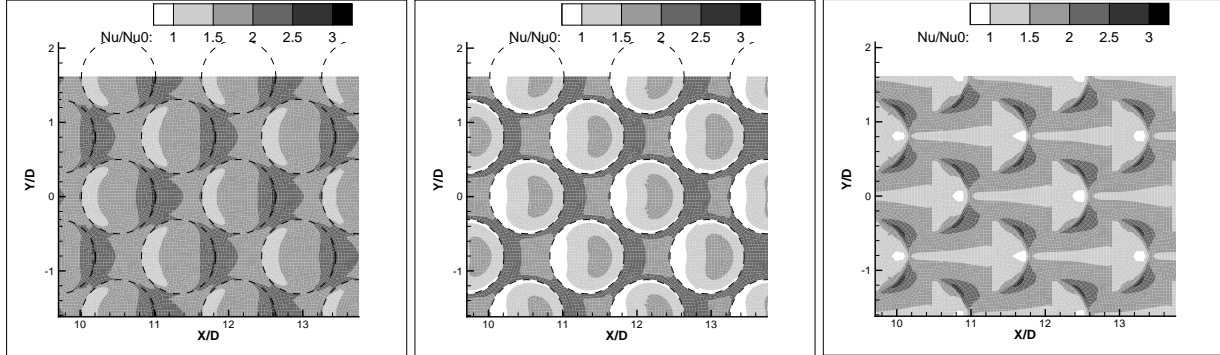


Figure 16: Nusselt Number for different dimple shape : spherical (left), cylinder (center), half cylinder (right)

#### 4. Thermal performance

A useful indicator to evaluate the cooling effectiveness of a device is the global thermal performance. This is the ratio of the mean spatial Nusselt number to the cube root mean friction :  $\eta = \frac{Nu/Nu_0}{(f/f_0)^{1/3}}$ . To evaluate the baseline friction, the Drew correlation  $f_0 = 0.00140 + 0.125Re^{-0.32}$  has been used, and the friction  $f$  can be directly linked to the pressure loss by the relation  $f = \frac{H\Delta P}{\rho U^2 \Delta x}$ . The results for the several cases computed in this study are presented on the table 3. The name of the different geometries corresponds to shape\_channel height\_dimple depth. For example, SPH\_H1\_d0.2 reads "spherical dimples with channel height  $H/D=1$  and dimple depth  $\delta/D=0.2$ ".

Table 3: Thermal efficiency for the different geometries computed

Geometry	Reynolds	$Nu/Nu_0$	$f/f_0$	$\eta$
CYL_H1_d0.2	20000	1.53	1.145	1.46
DEM CYL_H1_d0.2	20000	1.652	2.672	1.187
SPH_H0.2_d0.2	20000	2.200	4.877	1.293
SPH_H1_d0.1	20000	1.291	1.718	1.075
SPH_H1_d0.2	10000	1.713	3.003	1.184
SPH_H1_d0.2	20000	1.861	3.244	1.254
SPH_H1_d0.2	50000	1.889	3.974	1.190
SPH_H1_d0.3	20000	1.851	3.626	1.201

These results are comforted by the values detailed in [12]. The most effective cooling configuration seems to be the one with the smaller height of channel, but it has been remarked above that this configuration is quite difficult to compute, and these results have to be taken with caution. This configuration is also the one with the higher friction factor ratio. The second most effective configuration is the baseline case 1, with a channel height equals to the diameter of the spherical shaped dimples and a depth for dimples equals to 0.2 times the diameter. This configuration has been always at the center of the comparisons made through this study, and seems to be one of the best compromise so far. Compared to LES results obtained by Bertier and Grenard with the CEDRE code [13] (based on experiments by Çakan, Casarsa and Arts [14, 15]) on a ribbed channel), these values for a high blockage ratio ribbed channel reads 1.93 for  $Nu/Nu_0$ , 21.5 for  $f/f_0$  and 0.7 for  $\eta$ . Thus, the same level of Nusselt number can be obtained with a dimpled channel with a radically lowered pressure loss, which is always interesting in term of global engine efficiency.

## **5. Conclusions**

This work was the first on these cooling devices at ONERA. The choice was made to compute three baseline configuration to evaluate the CEDRE code and observe how it reacts to this geometry. Once the behaviour of the code was known on these configuration, it was possible to evaluate the consequences of changing one parameter in a reasonable range. This was made with the Reynolds number, the dimple depth and the geometry of the dimples. This last point is really interesting because the shape, the repartition, the density of dimples on a plate is endless. An infinite number of geometries could be invented, from a simple one to a really sophisticated one. Another aspect is that these dimples are used to cool strong strained surfaces : an interesting study would also be to evaluate the influence of dimple depth and shape in terms of structural behaviour for the materials.

## **Aknoledgements**

This work was supported by DGA (Délégation générale pour l'armement) in the scope of a general propulsion program.

## References

- [1] Mahmood, G.I. and Ligrani, P.M. Heat transfer in a dimpled channel: combined influences of aspect ratio, temperature ratio, Reynolds number and flow structure. In *International Journal of Heat and Mass Transfer*, Vol. 45, No 10, pp. 2011-2020, 2002.
- [2] Ligrani, P.M. and Burgess, N.K. and Won, S.Y. Nusselt numbers and flow structure on and above a shallow dimpled surface within a channel including effects of inlet turbulence intensity level. In *ASME Paper GT2004-54231*, pp. 1-13, 2004.
- [3] Burgess, N.K. and Ligrani, P.M. Effects of dimple depth on Nusselt numbers and friction factors for internal cooling in a channel. In *ASME Paper GT2004-54232*, pp. 1-10, 2004.
- [4] Moon, S.W. and Lau, S.C. Turbulent heat transfer measurements on a wall with concave and cylindrical dimples in a square channel. In *ASME Paper GT-2002-30208*, pp. 1-9, 2002.
- [5] Chyu, M.K. and Yu, Y. and Ding, H. and Downs, J.P. and Soechting, F.O. Concavity enhanced heat transfer in an internal cooling passage. In *ASME Paper 97-GT-437*, pp.1-6, 1997.
- [6] Ligrani, P.M. and Harrison, J.L. and Mahmood, G.I. and Hill, M.L. Flow structure due to dimple depression on a channel surface. In *Physics of Fluids*, Vol.13, No11, pp. 3442-3451, 2001.
- [7] Lin, Y.L. and Shih, T.I-P. and Chyu, M.K. Computations of flow and heat transfer in a channel with rows of hemispherical cavities. In *ASME Paper 99-GT-263*, pp. 1-6, 1999.
- [8] Park, J. and Desam, P.R. and Ligrani, P.M. Numerical predictions of flow structure above a dimpled surface in a channel. In *Numerical Heat Transfer, Part A*, 45:1-20, 2004.
- [9] Park, J. and Ligrani, P.M. Numerical predictions of heat transfer and fluid characteristics for seven different dimpled surfaces in a channel. In *Numerical Heat Transfer Part A*, 47:209-232, 2005.
- [10] Won, S.Y. and Ligrani, P.M. Numerical predictions of flow structure and local nusselt number ratios along and above dimpled surfaces with different dimple depths in a channel. In *3<sup>rd</sup> Numerical Heat Transfer Part A*, 46:549-570, 2004
- [11] Mahmood, G.I. and Hill, M.L. and Nelson, D.L. and Ligrani, P.M. and Moon, H.K. and Glezer, B. Local heat transfer and flow structure on and above a dimpled surface in a channel. In *Journal of Turbomachinery*, Vol. 123 No 1, pp. 115-123, 2001.
- [12] Ligrani, P.M. and Oliveira, M.M. and Blaskovich, T. Comparison of heat transfer augmentation techniques. In *AIAA Journal*, Vol. 41 No 3, pp. 337-362, 2003.
- [13] Bertier, N. Simulation des grandes échelles en aérothermique sur des maillages non-structurés généraux. PhD Thesis, ONERA, 2006.
- [14] Çakan, M. Aero-thermal Investigation of fixed Rib-roughened Internal Cooling Passage. *PhD thesis*, Von Karman Institute for Fluid Dynamics, 2000.
- [15] Casarsa, L. Aerodynamic Performance Investigation of fixed Rib-roughened Internal Cooling Passage. *PhD thesis*, Von Karman Institute for Fluid Dynamics, 2003.



**This page has been purposely left blank**